

# g-C<sub>3</sub>N<sub>4</sub> Photocatalysts

Subjects: Materials Science, Coatings & Films

Contributor: Junxiang Pei, Haofeng Li, Songlin Zhuang, Dawei Zhang, Dechao Yu

Graphitized carbon nitride (g-C<sub>3</sub>N<sub>4</sub>), as a metal-free, visible-light-responsive photocatalyst, has a very broad application prospect in the fields of solar energy conversion and environmental remediation. The g-C<sub>3</sub>N<sub>4</sub> photocatalyst owns a series of conspicuous characteristics, such as very suitable band structure, strong physicochemical stability, abundant reserves, low cost, etc. Research on the g-C<sub>3</sub>N<sub>4</sub> or g-C<sub>3</sub>N<sub>4</sub>-based photocatalysts for real applications has become a competitive hot topic and a frontier area with thousands of publications over the past 17 years.

Keywords: photocatalyst ; g-C<sub>3</sub>N<sub>4</sub> ; reaction parameters ; structure design ; exfoliation

## 1. Introduction

Recently, graphitic carbon nitride (g-C<sub>3</sub>N<sub>4</sub>) has attracted extremely wide attentions in photocatalysis due to its special band structure, stable properties, low price, and easy preparation [1][2][3][4][5]. The g-C<sub>3</sub>N<sub>4</sub> is comprised of only carbon and nitrogen elements, which are very abundant on the Earth. Importantly, the g-C<sub>3</sub>N<sub>4</sub> materials can be easily fabricated by thermal polymerization of abundant nitrogen-rich precursors such as melamine [6][7][8][9][10][11][12][13][14][15], dicyandiamide [16][17][18][19][20][21], cyanamide [22][23][24], urea [17][25][26], thiourea [27][28][29], ammonium thiocyanate [30][31][32], etc. Because the band gap of g-C<sub>3</sub>N<sub>4</sub> is 2.7 eV, it can absorb visible light shorter than 450 nm effectively, implying broad prospects in solar energy conversion applications. Due to the aromatic C-N heterocycles, g-C<sub>3</sub>N<sub>4</sub> is thermally stable up to 600 °C in air. Moreover, g-C<sub>3</sub>N<sub>4</sub> is insoluble in acids, bases or organic solvents, exhibiting good chemical stability.

However, some bottlenecks in the photocatalytic activity of g-C<sub>3</sub>N<sub>4</sub> still exist, such as fast photogenerated carrier recombination, limited active site, small specific surface area, low light absorption capacity, unsatisfactory crystallinity and unignorable surface defects. How to promote the efficient migration and separation of photogenerated carriers, expand the spectral response range and increase the specific surface area of g-C<sub>3</sub>N<sub>4</sub> is the core problem to achieve high energy conversion efficiency. In practice, the introduction of impurities into the g-C<sub>3</sub>N<sub>4</sub> matrix through copolymerization and doping has become an effective strategy to change the electronic structure and band structure of g-C<sub>3</sub>N<sub>4</sub>. On the other hand, numerous research works have demonstrated that the physicochemical properties and photocatalytic efficiency of the polymer g-C<sub>3</sub>N<sub>4</sub> can be significantly improved by optimizing synthesis techniques such as supramolecular and copolymerization techniques with identical structural and nano-structural designs, or by template-assisted methods to improve porosity and surface area [33][34][35][36][37][38]. Amongst various modification approaches, designing and constructing a more suitable band structure is the most important prerequisite to improve the charge separation efficiency, thereby enhancing the photocatalytic performance.

## 2. Influence of Synthesis Parameters

### 2.1. Precursors and Reaction Temperature

The first reported g-C<sub>3</sub>N<sub>4</sub> as a heterogeneous catalysis was present in 2006 [39]. Subsequently, various precursors such as urea [40], thiourea [41], cyanamide [42][43] and dicyandiamide [44][45] have been employed to synthesize g-C<sub>3</sub>N<sub>4</sub> by thermal treatment methods. In 2009, Wang et al. firstly used cyanamide as the precursor of g-C<sub>3</sub>N<sub>4</sub> for producing hydrogen from water under visible-light irradiation in the presence of a sacrificial donor [46]. This pioneering work represents an important first step towards photosynthesis in general, where artificial conjugated polymer semiconductors can be used as energy transducers. In order to demonstrate the reaction intermediate compounds, characterization techniques such as thermogravimetric analysis (TGA) and X-ray diffraction (XRD) are used to characterize the reaction. **Figure 1a** displayed that the graphitic planes are constructed from tri-s-triazine units connected by planar amino groups. **Figure 1b** is the XRD pattern of the obtained g-C<sub>3</sub>N<sub>4</sub> powder. From the ultraviolet-visible spectrum (**Figure 1c**), it can be seen that the band gap of g-C<sub>3</sub>N<sub>4</sub> is 2.7 eV. The synthesis of g-C<sub>3</sub>N<sub>4</sub> was a combination of polyaddition and polycondensation. At a reaction temperature of 203 and 234 °C, the cyanamide molecules can be condensed to dicyandiamide and melamine, respectively. The ammonia is then removed by condensation. When the temperature

reaches 335 °C, large amounts of melamine products are detected. When further heating to 390 °C, the rearrangements of melamine will result in the formation of tri-s-triazine units. Finally, when heating to 520 °C, the polymeric g-C<sub>3</sub>N<sub>4</sub> are synthesized via the further condensation of the unit. However, g-C<sub>3</sub>N<sub>4</sub> will be unstable at above 600 °C. **Figure 1d** shows the structural phase transition process from cyanamide to g-C<sub>3</sub>N<sub>4</sub> at different temperatures. In addition to in-situ characterization experiments to verify the reaction process, it can also be demonstrated by relevant simulation calculations. The first-principles DFT calculations were performed using a plane wave basis set with a 550 eV energy cutoff [39]. The calculation results showed that the cohesion energy increased under the addition of multiple reaction pathways, which confirmed that melamine was produced upon heating the cyanamide, as shown in **Figure 1e**.

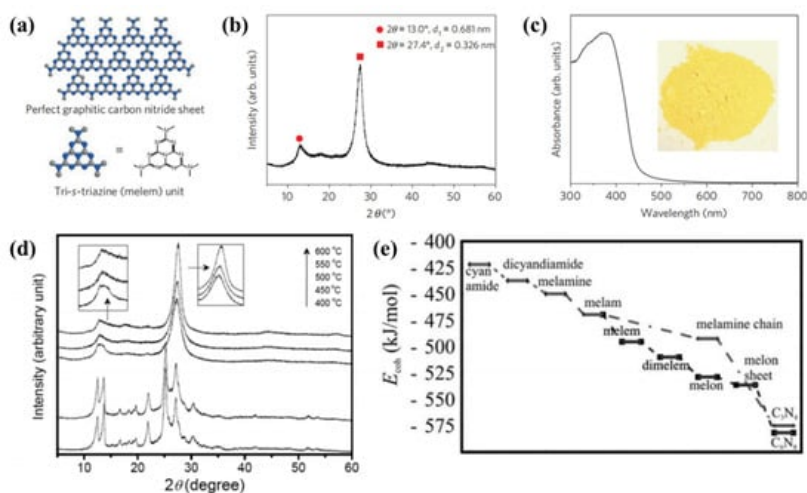


**Figure 1.** Crystal structure and optical properties of g-C<sub>3</sub>N<sub>4</sub>. (a) Schematic diagram of a perfect g-C<sub>3</sub>N<sub>4</sub> sheet constructed from melam units. (b) Experimental XRD pattern of polymeric carbon nitride, revealing a graphitic structure with an interplanar stacking distance of the aromatic unit (0.326 nm). (c) Diffuse reflectance spectrum of the polymeric carbon nitride. Inset: Photograph of the photocatalyst. (d) XRD patterns of g-C<sub>3</sub>N<sub>4</sub> treated at different temperatures. (e) Calculated energy diagram for the development of g-C<sub>3</sub>N<sub>4</sub> using cyanamide precursor [46].

## 2.2. C/N Ratio

Generally, g-C<sub>3</sub>N<sub>4</sub> exhibits a high physicochemical stability and ideal band structure, due to the high condensation degree and the presence of the heptazine ring structure. When the appropriate precursor and condensation method are selected, the C/N ratio in layered g-C<sub>3</sub>N<sub>4</sub> is about 0.75. Many studies have confirmed that when the precursors and synthesis parameters of g-C<sub>3</sub>N<sub>4</sub> are changed, the physicochemical properties of g-C<sub>3</sub>N<sub>4</sub> will be significantly affected, such as band gap width, specific surface area, C/N ratio, etc., which will directly affect the photocatalytic efficiency and other applications' performance [47][48][49][50][51]. Yan et al. synthesized g-C<sub>3</sub>N<sub>4</sub> by directly heating the low-cost melamine, and they change the C/N ratio by controlling different heating temperatures [52]. The research showed that when the heating temperatures increased from 500 to 580 °C, the ratio of C/N increased from 0.721 to 0.742. Meanwhile, the band gaps of g-C<sub>3</sub>N<sub>4</sub> decreased from 2.8 to 2.75 eV.

## 2.3. Pretreatment of Precursors

It has been shown that modification and pretreatment of nitrogen-rich precursors before thermal annealing can effectively improve the physicochemical properties of g-C<sub>3</sub>N<sub>4</sub>. One of the effective pretreatment methods is by acid treatment. Yan et al. reported the synthesis of g-C<sub>3</sub>N<sub>4</sub> by directly heating the sulfuric-acid-treated melamine precursor [53]. It is worth noting that the carbon nitride synthesized from sulfuric acid treated melamine (15.6 m<sup>2</sup>/g) shows relatively higher BET surface area than that of samples synthesized from untreated melamine (8.6 m<sup>2</sup>/g). The reason can be attributed to the effect of pretreatment of melamine with H<sub>2</sub>SO<sub>4</sub> on its condensation process, during which sublimation of melamine is inhibited significantly. In addition to the pretreatment of melamine with H<sub>2</sub>SO<sub>4</sub>, HCl and HNO<sub>3</sub> also exhibited good pretreatment effects on melamine [54][55][56][57].

In addition to acid precursors, pretreatment methods of sulfur-mediated synthesis can also be used to regulate the structure and physicochemical properties of g-C<sub>3</sub>N<sub>4</sub> [58]. The fundamental reason is that the presence of the sulfur group in the sulfur-containing thiourea provides an additional chemical pathway to regulate the degree of condensation and polymerization of g-C<sub>3</sub>N<sub>4</sub> because it is easy to leave the -SH groups.

## 2.4. Reaction Atmosphere

In addition to the types of precursors, reaction temperature and duration, the physicochemical properties and structure of g-C<sub>3</sub>N<sub>4</sub> are also strongly influenced by the reaction atmosphere, because the reaction atmosphere can induce a variety of defects and carbon and nitrogen vacancies. In fact, defects are essential for catalytic reactions because they can act as active sites for reactant molecules and change the band structure by introducing additional energy levels in the forbidden band, thus extending the spectral absorption range [59][60][61][62]. By controlling the polycondensation temperature of a dicyandiamide precursor in the preparation of g-C<sub>3</sub>N<sub>4</sub>, Niu et al. introduced nitrogen vacancies in the framework of g-C<sub>3</sub>N<sub>4</sub> [63]. The excess electrons caused by nitrogen loss in g-C<sub>3</sub>N<sub>4</sub> lead to a large number of C<sup>3+</sup> states associated with nitrogen vacancies in the band gap, thus reducing the intrinsic band gap from 2.74 eV to 2.66 eV. Steady and time-resolved fluorescence emission spectra show that, due to the existence of abundant nitrogen vacancies, the intrinsic radiative recombination of electrons and holes in g-C<sub>3</sub>N<sub>4</sub> is greatly restrained, and the population of short-lived and long-lived charge carriers is decreased and increased, respectively.

## 3. Morphology and Structure Design of g-C<sub>3</sub>N<sub>4</sub>

### 3.1. Hard and Soft Template Approach

Apart from regulating the synthesis parameters, introducing nano-templates and nano-casting with different morphology and ordered porosity on the basis of bulk g-C<sub>3</sub>N<sub>4</sub> is another promising method to change the morphology and structural characteristics of g-C<sub>3</sub>N<sub>4</sub> structure and the interlayer interaction. As a matter of fact, researchers have effectively designed controllable nanostructures for g-C<sub>3</sub>N<sub>4</sub> through hard template or soft template methods, such as porous g-C<sub>3</sub>N<sub>4</sub>, one-dimensional nanostructures, hollow g-C<sub>3</sub>N<sub>4</sub> nanospheres, etc [10][64][65][66][67][68][69][70][71][72]. It has been proven that the porosity, structure, morphology, surface area and size can be easily controlled by adjusting the appropriate template. Moreover, the larger surface area and more active sites are generally more favorable for photocatalytic applications of g-C<sub>3</sub>N<sub>4</sub>.

The hard template method is almost identical to the traditional casting process and is one of the most common techniques for developing nanostructured g-C<sub>3</sub>N<sub>4</sub> materials. In this way, the various structures and geometries of g-C<sub>3</sub>N<sub>4</sub> can be designed using hard templates as needed, and their length scales are usually around nanometers and microns. The most typical structure-oriented agent is a silica template with a controllable nanostructure. The early study on the mesoporous g-C<sub>3</sub>N<sub>4</sub> synthesized using cyanamide as a precursor and silica nanoparticles with a size of 12 nm as a template was reported by Goettmann et al. [39]. The results show that the silica nanoparticles can be uniformly dispersed in the cyanamide monomer, which is due to the appropriate surface interaction between the silica surface and the amine and aromatic nitrogen groups.

It can be seen that during the synthesis of g-C<sub>3</sub>N<sub>4</sub> through hard templates, extremely dangerous, toxic and expensive fluorine-containing etchers (such as HF and NH<sub>4</sub>HF<sub>2</sub>) are used to remove the sacrificial templates. This greatly limits the practical application of the method in large-scale industrial processes. Therefore, apart from the hard template synthesis method of g-C<sub>3</sub>N<sub>4</sub>, the relatively “environmentally friendly” soft template process can not only change the morphology and structure of g-C<sub>3</sub>N<sub>4</sub> through the selection of multiple soft templates, but also simplify the synthesis route of g-C<sub>3</sub>N<sub>4</sub> [73][74].

### 3.2. Supramolecular Preorganization Approach

In contrast to the previously discussed hard and soft template synthesis approaches, molecular self-assembly is a self-templating approach (namely supramolecular preorganization approach) in which molecules spontaneously form a stable g-C<sub>3</sub>N<sub>4</sub> structure from non-covalent bonds under equilibrium conditions in the absence of an external template [67][75][76][77]. Recently, supramolecular preassembly of triazine molecules has become an interesting method to regulate the structural, textural, optical, and electronic features of g-C<sub>3</sub>N<sub>4</sub>, thus affecting its photocatalytic activity [78][79][80][81]. For example, nanostructured g-C<sub>3</sub>N<sub>4</sub> materials can be developed by supramolecular preorganization of melamine precursors to triazine derivatives to form hydrogen bond molecular assemblies, i.e., melamine–cyanuric acid, melamine–trithiocyanuric acid mixtures or their derivatives [82][83][84].

It can be seen that the combination of two or more monomers in different solvents can form supramolecular complexes. These supramolecular complexes are usually linked by hydrogen bonds. Therefore, it is expected that the addition of new monomers to hydrogen-bonded supramolecular complexes as “terminators” will be an attractive technique to further adjust the morphology, photophysical properties, and electronic band structure of g-C<sub>3</sub>N<sub>4</sub>.

### 3.3. Template-Free Approach

Compared with the hard and soft template synthesis approaches, the template-free approach has unique advantages, such as no need for various high-cost and dangerous templates containing fluorine, and no residue of any template components. Indeed, many studies have proven that g-C<sub>3</sub>N<sub>4</sub> nanostructure designs with a variety of morphologies and desired sizes, such as nanorods, quantum dots, microspheres, nanofibers, etc., can also be achieved using a template-free approach. Bai et al. reported that the transformation of g-C<sub>3</sub>N<sub>4</sub> from nanoplates to nanorods was realized by a simple reflux method [85].

Additionally, Wang et al. described a facile and generally feasible method to synthesize nanotube-type g-C<sub>3</sub>N<sub>4</sub> by directly heating melamine packed in an appropriate compact degree without templates [86]. A certain amount of melamine was placed into a semi-closed alumina crucible followed by consecutively shaking the crucible using a vibrator at a fast rate to achieve a moderately compact packing degree. This process is very crucial for the synthesis of nanotube-type g-C<sub>3</sub>N<sub>4</sub>. TEM images show that the wall thickness of the nanotubes in the bulk phase is about 15 ± 2 nm, while the inner diameter is about 18 ± 2 nm. During the pyrolysis process, melamine releases NH<sub>3</sub> gas, which passes through the stacked melamine layers to form rolled g-C<sub>3</sub>N<sub>4</sub> nanosheets.

## 4. Exfoliation of Bulk g-C<sub>3</sub>N<sub>4</sub>

Although the specific surface area of the monolayer g-C<sub>3</sub>N<sub>4</sub> is theoretically large, the specific surface area of the block is very low indeed, usually less than 10 m<sup>2</sup> g<sup>-1</sup>, due to the stacking of g-C<sub>3</sub>N<sub>4</sub> layers [87]. Therefore, delaminating g-C<sub>3</sub>N<sub>4</sub> into several layers is a promising way to improve photocatalytic performance and produce more interesting surface, optical and electronic properties [88][89][90][91]. There are many methods of exfoliating g-C<sub>3</sub>N<sub>4</sub>, such as ultrasonication-assisted liquid exfoliation, the liquid ammonia-assisted lithiation and the post-thermal oxidation etching route [16][90][91][92][93][94][95][96][97].

Liquid exfoliation is simple and convenient, and has gradually become the most commonly used exfoliation method by most researchers. Yang et al. demonstrated the synthesis of free-standing g-C<sub>3</sub>N<sub>4</sub> nanosheets by liquid phase exfoliation [92]. The method uses g-C<sub>3</sub>N<sub>4</sub> powder as a starting material and various organic solvents (such as isopropanol (IPA), N-methyl-pyrrolidone (NMP), acetone, and ethanol) as dispersing media.

## 5. Doping of g-C<sub>3</sub>N<sub>4</sub>

It is well-known that g-C<sub>3</sub>N<sub>4</sub> is a metal-free n-type semiconductor. Due to the high ionization energy and high electronegativity of metal-free semiconductors, it is easy for them to form covalent bonds with other compounds by obtaining electrons during the reaction. In order to maintain this unique advantage of metal-free semiconductors, researchers have implemented a series of non-metal doping g-C<sub>3</sub>N<sub>4</sub>, including oxygen, phosphorus, sulfur, carbon, halogen, nitrogen and boron [98][99][100][101][102][103]. For instance, O-doping is a facile method to improve the photocatalytic ability of g-C<sub>3</sub>N<sub>4</sub>. Zeng et al. synthesized one-dimensional porous architectural g-C<sub>3</sub>N<sub>4</sub> nanorods by direct calcination of hydrous melamine nanofibers precipitated from an aqueous solution of melamine [104]. The porous structure increases the specific surface area, enhances the light absorption capacity and improves the catalytic reaction rate. At the same time, doping oxygen atoms into the g-C<sub>3</sub>N<sub>4</sub> matrix breaks the symmetry of the pristine structure, making more efficient separation of electron/hole pairs. In general, non-metallic doping usually changes the surface morphology and structure of g-C<sub>3</sub>N<sub>4</sub>, thereby affecting the light absorption efficiency and regulating the catalytic efficiency.

## 6. Applications of g-C<sub>3</sub>N<sub>4</sub>

Due to its moderate energy gap, excellent electronic properties, rich functional groups and surface defects, g-C<sub>3</sub>N<sub>4</sub> can be widely used in environmental treatment and pollutant degradation, including water splitting, hydrogen generation, CO<sub>2</sub> conversion and organic pollutants degradation [105][106][107][108].

As reported, the pristine g-C<sub>3</sub>N<sub>4</sub> has limitations such as small specific surface area and fast charge recombination rate, which leads to a low water splitting ability of g-C<sub>3</sub>N<sub>4</sub>. To solve this problem, Chen et al. improved the water splitting capacity via adjusting the dimension of g-C<sub>3</sub>N<sub>4</sub> [109]. As shown in **Figure 2a,b**, they demonstrated that the evolution rates of H<sub>2</sub> and O<sub>2</sub> of three-dimensional porous g-C<sub>3</sub>N<sub>4</sub> in visible light are significantly higher than those of the pristine g-C<sub>3</sub>N<sub>4</sub>, reaching 101.4 and 49.1 μmol g<sup>-1</sup> h<sup>-1</sup>, respectively. Fu et al. reported oxygen-doped g-C<sub>3</sub>N<sub>4</sub> [110]. As exhibited in **Figure 2c-d**, the O-doped g-C<sub>3</sub>N<sub>4</sub> has a narrower band gap and greater CO<sub>2</sub> affinity, which significantly improves the photogenerated carrier separation efficiency and CO<sub>2</sub> conversion ability. In addition, a lot of efforts have been made to

enhance its photocatalytic activity to improve its pollutant degradation ability. As shown in **Figure 2e-f**, Dou et al. reported that mesoporous g-C<sub>3</sub>N<sub>4</sub> has a strong ability to remove antibiotics under visible light [111], which is mainly due to the porous structure that improved the utilization of light.

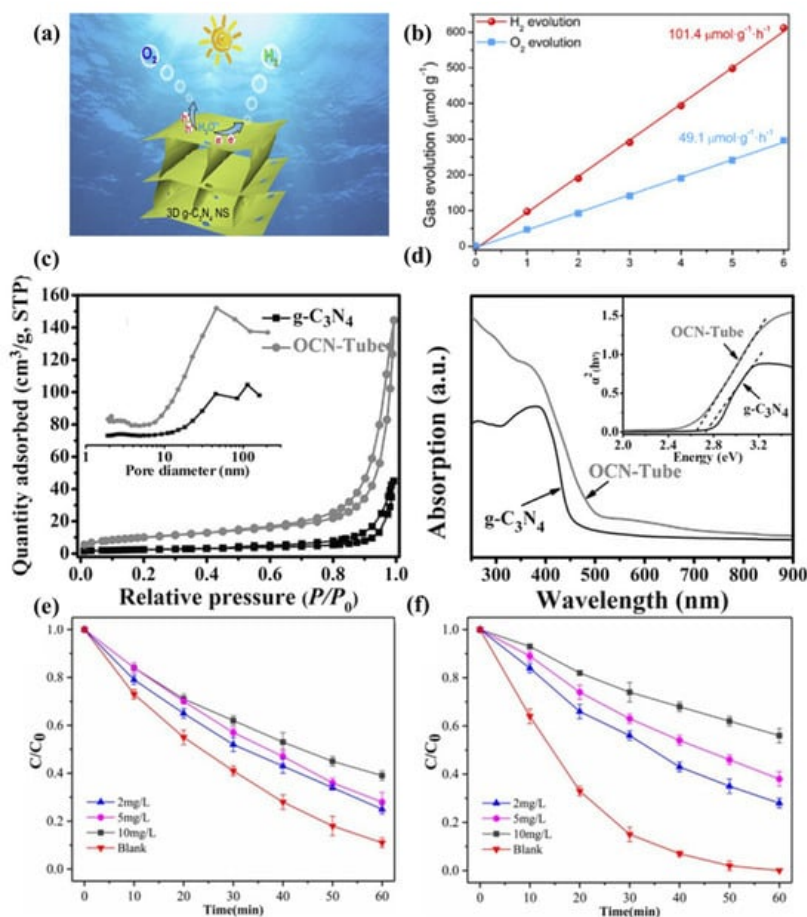


**Figure 2.** (a) Water splitting for H<sub>2</sub> and O<sub>2</sub> Evolution. (b) Time-dependent overall water splitting over 3D g-C<sub>3</sub>N<sub>4</sub> [109]. (c) N<sub>2</sub> adsorption-desorption isotherms and corresponding pore size distribution curves. (d) UV-vis diffuse reflectance spectra [110]. The effects of humic acid on (e) amoxicillin and (f) cefotaxime photodegradation by mesoporous carbon nitride (initial pH = 7) [111].

## 7. Conclusions

In summary, due to the merits of low cost, high stability and visible light response, g-C<sub>3</sub>N<sub>4</sub> is one of the most promising photocatalytic materials to replace TiO<sub>2</sub>. As summarized above, the appropriate reaction temperature and duration of the condensation process are beneficial to improve the crystallinity of g-C<sub>3</sub>N<sub>4</sub>. Various desirable nanostructures of g-C<sub>3</sub>N<sub>4</sub> can be constructed via hard and soft template approaches, supramolecular preorganization approach, and template-free approach. Liquid exfoliation of bulk g-C<sub>3</sub>N<sub>4</sub> has becoming the most facile and promising method to improve the surface area of g-C<sub>3</sub>N<sub>4</sub>.

Therefore, in order to synthesize the ideal g-C<sub>3</sub>N<sub>4</sub> with high photocatalytic efficiency, it is necessary to pay attention to the following crucial elements: (i) Controlling the corresponding reaction temperature and reaction time according to the selected precursor material; (ii) Controlling the C/N ratio close to 0.75 and the band gap to 2.7 eV; (iii) Extending the specific surface area by selecting suitable nanostructure design approaches.

## References

- Xu, M.-L.; Lu, M.; Qin, G.-Y.; Wu, X.-M.; Yu, T.; Zhang, L.-N.; Li, K.; Cheng, X.; Lan, Y.-Q. Piezo-Photocatalytic Synergy in BiFeO<sub>3</sub>@COF Z-Scheme Heterostructures for High-Efficiency Overall Water Splitting. *Angew. Chem.-Int. Ed.* 2022, 61, e202210700.
- Miao, Z.; Wang, Q.; Zhang, Y.; Meng, L.; Wang, X. In situ construction of S-scheme AgBr/BiOBr heterojunction with surface oxygen vacancy for boosting photocatalytic CO<sub>2</sub> reduction with H<sub>2</sub>O. *Appl. Catal. B-Environ.* 2022, 301, 120802.

3. Peng, X.; Wu, J.; Zhao, Z.; Wang, X.; Dai, H.; Wei, Y.; Xu, G.; Hu, F. Activation of peroxymonosulfate by single atom Co-N-C catalysts for high-efficient removal of chloroquine phosphate via non-radical pathways: Electron-transfer mechanism. *Chem. Eng. J.* 2022, 429, 132245.
4. Bai, J.; Shen, R.; Jiang, Z.; Zhang, P.; Li, Y.; Li, X. Integration of 2D layered CdS/WO<sub>3</sub> S-scheme heterojunctions and metallic Ti<sub>3</sub>C<sub>2</sub> MXene-based Ohmic junctions for effective photocatalytic H<sub>2</sub> generation. *Chin. J. Catal.* 2022, 43, 359–369.
5. Chen, T.; Yu, K.; Dong, C.; Yuan, X.; Gong, X.; Lian, J.; Cao, X.; Li, M.; Zhou, L.; Hu, B.; et al. Advanced photocatalysts for uranium extraction: Elaborate design and future perspectives. *Coord. Chem. Rev.* 2022, 467, 214615.
6. Guo, S.; Deng, Z.; Li, M.; Jiang, B.; Tian, C.; Pan, Q.; Fu, H. Phosphorus-Doped Carbon Nitride Tubes with a Layered Micro-nanostructure for Enhanced Visible-Light Photocatalytic Hydrogen Evolution. *Angew. Chem.-Int. Ed.* 2016, 55, 1830–1834.
7. Guo, S.; Tang, Y.; Xie, Y.; Tian, C.; Feng, Q.; Zhou, W.; Jiang, B. P-doped tubular g-C<sub>3</sub>N<sub>4</sub> with surface carbon defects: Universal synthesis and enhanced visible-light photocatalytic hydrogen production. *Appl. Catal. B-Environ.* 2017, 218, 664–671.
8. Liu, H.; Chen, D.; Wang, Z.; Jing, H.; Zhang, R. Microwave-assisted molten-salt rapid synthesis of isotype triazine/heptazine based g-C<sub>3</sub>N<sub>4</sub> heterojunctions with highly enhanced photocatalytic hydrogen evolution performance. *Appl. Catal. B-Environ.* 2017, 203, 300–313.
9. Mo, Z.; Xu, H.; Chen, Z.; She, X.; Song, Y.; Wu, J.; Yan, P.; Xu, L.; Leia, Y.; Yuan, S.; et al. Self-assembled synthesis of defect-engineered graphitic carbon nitride nanotubes for efficient conversion of solar energy. *Appl. Catal. B-Environ.* 2018, 225, 154–161.
10. Zhang, J.-W.; Gong, S.; Mahmood, N.; Pan, L.; Zhang, X.; Zou, J.-J. Oxygen-doped nanoporous carbon nitride via water-based homogeneous supramolecular assembly for photocatalytic hydrogen evolution. *Appl. Catal. B-Environ.* 2018, 221, 9–16.
11. Zhu, B.; Xia, P.; Ho, W.; Yu, J. Isoelectric point and adsorption activity of porous g-C<sub>3</sub>N<sub>4</sub>. *Appl. Surf. Sci.* 2015, 344, 188–195.
12. Huang, H.; Xiao, K.; Tian, N.; Dong, F.; Zhang, T.; Du, X.; Zhang, Y. Template-free precursor-surface-etching route to porous, thin g-C<sub>3</sub>N<sub>4</sub> nanosheets for enhancing photocatalytic reduction and oxidation activity. *J. Mater. Chem. A* 2017, 5, 17452–17463.
13. Tian, N.; Zhang, Y.; Li, X.; Xiao, K.; Du, X.; Dong, F.; Waterhouse, G.I.N.; Zhang, T.; Huang, H. Precursor-reforming protocol to 3D mesoporous g-C<sub>3</sub>N<sub>4</sub> established by ultrathin self-doped nanosheets for superior hydrogen evolution. *Nano Energy* 2017, 38, 72–81.
14. Wang, X.; Zhou, C.; Shi, R.; Liu, Q.; Waterhouse, G.I.N.; Wu, L.; Tung, C.-H.; Zhang, T. Supramolecular precursor strategy for the synthesis of holey graphitic carbon nitride nanotubes with enhanced photocatalytic hydrogen evolution performance. *Nano Res.* 2019, 12, 2385–2389.
15. Zhou, C.; Shi, R.; Shang, L.; Wu, L.-Z.; Tung, C.-H.; Zhang, T. Template-free large-scale synthesis of g-C<sub>3</sub>N<sub>4</sub> microtubes for enhanced visible light-driven photocatalytic H<sub>2</sub> production. *Nano Res.* 2018, 11, 3462–3468.
16. Han, Q.; Wang, B.; Gao, J.; Cheng, Z.; Zhao, Y.; Zhang, Z.; Qu, L. Atomically Thin Mesoporous Nanomesh of Graphitic C<sub>3</sub>N<sub>4</sub> for High-Efficiency Photocatalytic Hydrogen Evolution. *Acs Nano* 2016, 10, 2745–2751.
17. Yang, P.; Ou, H.; Fang, Y.; Wang, X. A Facile Steam Reforming Strategy to Delaminate Layered Carbon Nitride Semiconductors for Photoredox Catalysis. *Angew. Chem.-Int. Ed.* 2017, 56, 3992–3996.
18. Lan, Z.-A.; Zhang, G.; Wang, X. A facile synthesis of Br-modified g-C<sub>3</sub>N<sub>4</sub> semiconductors for photoredox water splitting. *Appl. Catal. B-Environ.* 2016, 192, 116–125.
19. Zhang, M.; Bai, X.; Liu, D.; Wang, J.; Zhu, Y. Enhanced catalytic activity of potassium-doped graphitic carbon nitride induced by lower valence position. *Appl. Catal. B-Environ.* 2015, 164, 77–81.
20. Hu, S.; Ma, L.; You, J.; Li, F.; Fan, Z.; Lu, G.; Liu, D.; Gui, J. Enhanced visible light photocatalytic performance of g-C<sub>3</sub>N<sub>4</sub> photocatalysts co-doped with iron and phosphorus. *Appl. Surf. Sci.* 2014, 311, 164–171.
21. Hu, S.; Li, F.; Fan, Z.; Wang, F.; Zhao, Y.; Lv, Z. Band gap-tunable potassium doped graphitic carbon nitride with enhanced mineralization ability. *Dalton Trans.* 2015, 44, 1084–1092.
22. Lan, H.; Li, L.; An, X.; Liu, F.; Chen, C.; Liu, H.; Qu, J. Microstructure of carbon nitride affecting synergetic photocatalytic activity: Hydrogen bonds vs. structural defects. *Appl. Catal. B-Environ.* 2017, 204, 49–57.
23. Shen, Y.; Guo, X.; Bo, X.; Wang, Y.; Guo, X.; Xie, M.; Guo, X. Effect of template-induced surface species on electronic structure and photocatalytic activity of g-C<sub>3</sub>N<sub>4</sub>. *Appl. Surf. Sci.* 2017, 396, 933–938.

24. Perez-Molina, A.; Pastrana-Martinez, L.M.; Morales-Torres, S.; Maldonado-Hodar, F.J. Photodegradation of cytostatic drugs by g-C<sub>3</sub>N<sub>4</sub>: Synthesis, properties and performance fitted by selecting the appropriate precursor. *Catal. Today* 2023, 418, 114068.
25. Gao, Y.; Zhu, Y.; Lyu, L.; Zeng, Q.; Xing, X.; Hu, C. Electronic Structure Modulation of Graphitic Carbon Nitride by Oxygen Doping for Enhanced Catalytic Degradation of Organic Pollutants through Peroxymonosulfate Activation. *Environ. Sci. Technol.* 2018, 52, 14371–14380.
26. Fang, J.; Fan, H.; Li, M.; Long, C. Nitrogen self-doped graphitic carbon nitride as efficient visible light photocatalyst for hydrogen evolution. *J. Mater. Chem. A* 2015, 3, 13819–13826.
27. Yu, H.; Shi, R.; Zhao, Y.; Bian, T.; Zhao, Y.; Zhou, C.; Waterhouse, G.I.N.; Wu, L.-Z.; Tung, C.-H.; Zhang, T. Alkali-Assisted Synthesis of Nitrogen Deficient Graphitic Carbon Nitride with Tunable Band Structures for Efficient Visible-Light-Driven Hydrogen Evolution. *Adv. Mater.* 2017, 29, 1605148.
28. Li, X.; Zhang, J.; Huo, Y.; Dai, K.; Li, S.; Chen, S. Two-dimensional sulfur- and chlorine-codoped g-C<sub>3</sub>N<sub>4</sub>/CdSe-amine heterostructures nanocomposite with effective interfacial charge transfer and mechanism insight. *Appl. Catal. B-Environ.* 2021, 280, 119452.
29. Li, G.; Tang, Y.; Fu, T.; Xiang, Y.; Xiong, Z.; Si, Y.; Guo, C.; Jiang, Z. S, N co-doped carbon nanotubes coupled with CoFe nanoparticles as an efficient bifunctional ORR/OER electrocatalyst for rechargeable Zn-air batteries. *Chem. Eng. J.* 2022, 429, 132174.
30. Yu, B.; Shi, J.; Tan, S.; Cui, Y.; Zhao, W.; Wu, H.; Luo, Y.; Li, D.; Meng, Q. Efficient (>20%) and Stable All-Inorganic Cesium Lead Triiodide Solar Cell Enabled by Thiocyanate Molten Salts. *Angew. Chem.-Int. Ed.* 2021, 60, 13436–13443.
31. Su, Y.; Zhang, Y.; Zhuang, X.; Li, S.; Wu, D.; Zhang, F.; Feng, X. Low-temperature synthesis of nitrogen/sulfur co-doped three-dimensional graphene frameworks as efficient metal-free electrocatalyst for oxygen reduction reaction. *Carbon* 2013, 62, 296–301.
32. Zhang, L.; Xu, Z. A review of current progress of recycling technologies for metals from waste electrical and electronic equipment. *J. Clean. Prod.* 2016, 127, 19–36.
33. Ye, C.; Li, J.-X.; Li, Z.-J.; Li, X.-B.; Fan, X.-B.; Zhang, L.-P.; Chen, B.; Tung, C.-H.; Wu, L.-Z. Enhanced Driving Force and Charge Separation Efficiency of Protonated g-C<sub>3</sub>N<sub>4</sub> for Photocatalytic O<sub>2</sub> Evolution. *ACS Catal.* 2015, 5, 6973–6979.
34. Zhang, G.; Zang, S.; Wang, X. Layered Co(OH)<sub>2</sub> Deposited Polymeric Carbon Nitrides for Photocatalytic Water Oxidation. *ACS Catal.* 2015, 5, 941–947.
35. Hao, X.; Zhou, J.; Cui, Z.; Wang, Y.; Wang, Y.; Zou, Z. Zn-vacancy mediated electron-hole separation in ZnS/g-C<sub>3</sub>N<sub>4</sub> heterojunction for efficient visible-light photocatalytic hydrogen production. *Appl. Catal. B-Environ.* 2018, 229, 41–51.
36. Tang, J.-Y.; Guo, R.-T.; Zhou, W.-G.; Huang, C.-Y.; Pan, W.-G. Ball-flower like NiO/g-C<sub>3</sub>N<sub>4</sub> heterojunction for efficient visible light photocatalytic CO<sub>2</sub> reduction. *Appl. Catal. B-Environ.* 2018, 237, 802–810.
37. Zhang, H.; Zhao, L.; Geng, F.; Guo, L.-H.; Wan, B.; Yang, Y. Carbon dots decorated graphitic carbon nitride as an efficient metal-free photocatalyst for phenol degradation. *Appl. Catal. B-Environ.* 2016, 180, 656–662.
38. Wang, Z.; Guan, W.; Sun, Y.; Dong, F.; Zhou, Y.; Ho, W.-K. Water-assisted production of honeycomb-like g-C<sub>3</sub>N<sub>4</sub> with ultralong carrier lifetime and outstanding photocatalytic activity. *Nanoscale* 2015, 7, 2471–2479.
39. Goettmann, F.; Fischer, A.; Antonietti, M.; Thomas, A. Metal-free catalysis of sustainable Friedel-Crafts reactions: Direct activation of benzene by carbon nitrides to avoid the use of metal chlorides and halogenated compounds. *Chem. Commun.* 2006, 4530–4532.
40. Niu, Y.; Hu, F.; Xu, H.; Zhang, S.; Song, B.; Wang, H.; Li, M.; Shao, G.; Wang, H.; Lu, H. Exploration for high performance g-C<sub>3</sub>N<sub>4</sub> photocatalyst from different precursors. *Mater. Today Commun.* 2023, 34, 105040.
41. Thi Kim Anh, N.; Thanh-Truc, P.; Huy, N.-P.; Shin, E.W. The effect of graphitic carbon nitride precursors on the photocatalytic dye degradation of water-dispersible graphitic carbon nitride photocatalysts. *Appl. Surf. Sci.* 2021, 537, 148027.
42. Cardenas, A.; Vazquez, A.; Obregon, S.; Ruiz-Gomez, M.A.; Rodriguez-Gonzalez, V. New insights into the fluorescent sensing of Fe<sup>3+</sup> ions by g-C<sub>3</sub>N<sub>4</sub> prepared from different precursors. *Mater. Res. Bull.* 2021, 142, 111385.
43. Liu, X.; Xu, X.; Gan, H.; Yu, M.; Huang, Y. The Effect of Different g-C<sub>3</sub>N<sub>4</sub> Precursor Nature on Its Structural Control and Photocatalytic Degradation Activity. *Catalysts* 2023, 13, 848.
44. Catherine, H.N.; Chiu, W.-L.; Chang, L.-L.; Tung, K.-L.; Hu, C. Gel-like Ag-Dicyandiamide Metal-Organic Supramolecular Network-Derived g-C<sub>3</sub>N<sub>4</sub> for Photocatalytic Hydrogen Generation. *Acs Sustain. Chem. Eng.* 2022, 10,

45. Ren, X.; Yu, Q.; Pan, J.; Wang, Q.; Li, Y.; Shi, N. Photocatalytic degradation of methylene blue by C/g-C<sub>3</sub>N<sub>4</sub> composites formed by different carbon sources. *React. Kinet. Mech. Catal.* 2022, 135, 2279–2289.
46. Wang, X.; Maeda, K.; Thomas, A.; Takanabe, K.; Xin, G.; Carlsson, J.M.; Domen, K.; Antonietti, M. A metal-free polymeric photocatalyst for hydrogen production from water under visible light. *Nat. Mater.* 2009, 8, 76–80.
47. Xiao, H.; Wang, W.; Liu, G.; Chen, Z.; Lv, K.; Zhu, J. Photocatalytic performances of g-C<sub>3</sub>N<sub>4</sub> based catalysts for RhB degradation: Effect of preparation conditions. *Appl. Surf. Sci.* 2015, 358, 313–318.
48. Sun, T.; Li, C.; Bao, Y.; Fan, J.; Liu, E. S-Scheme MnCo<sub>2</sub>S<sub>4</sub>/g-C<sub>3</sub>N<sub>4</sub> Heterojunction Photocatalyst for H<sub>2</sub> Production. *Acta Phys.-Chim. Sin.* 2023, 39, 2212009.
49. Wang, J.; Wang, S. A critical review on graphitic carbon nitride (g-C<sub>3</sub>N<sub>4</sub>)-based materials: Preparation, modification and environmental application. *Coord. Chem. Rev.* 2022, 453, 214338.
50. Zhang, X.; Ma, P.; Wang, C.; Gan, L.; Chen, X.; Zhang, P.; Wang, Y.; Li, H.; Wang, L.; Zhou, X.; et al. Unraveling the dual defect sites in graphite carbon nitride for ultra-high photocatalytic H<sub>2</sub>O<sub>2</sub> evolution. *Energy Environ. Sci.* 2022, 15, 830–842.
51. Baladi, E.; Davar, F.; Hojjati-Najafabadi, A. Synthesis and characterization of g-C<sub>3</sub>N<sub>4</sub>-CoFe<sub>2</sub>O<sub>4</sub>-ZnO magnetic nanocomposites for enhancing photocatalytic activity with visible light for degradation of penicillin G antibiotic. *Environ. Res.* 2022, 215, 114270.
52. Yan, S.C.; Li, Z.S.; Zou, Z.G. Photodegradation Performance of g-C<sub>3</sub>N<sub>4</sub> Fabricated by Directly Heating Melamine. *Langmuir* 2009, 25, 10397–10401.
53. Yan, H.; Chen, Y.; Xu, S. Synthesis of graphitic carbon nitride by directly heating sulfuric acid treated melamine for enhanced photocatalytic H<sub>2</sub> production from water under visible light. *Int. J. Hydrogen Energy* 2012, 37, 125–133.
54. Dong, G.; Zhang, L. Porous structure dependent photoreactivity of graphitic carbon nitride under visible light. *J. Mater. Chem.* 2012, 22, 1160–1166.
55. Zhang, X.-S.; Hu, J.-Y.; Jiang, H. Facile modification of a graphitic carbon nitride catalyst to improve its photoreactivity under visible light irradiation. *Chem. Eng. J.* 2014, 256, 230–237.
56. Gao, J.; Zhou, Y.; Li, Z.; Yan, S.; Wang, N.; Zou, Z. High-yield synthesis of millimetre-long, semiconducting carbon nitride nanotubes with intense photoluminescence emission and reproducible photoconductivity. *Nanoscale* 2012, 4, 3687–3692.
57. Zhong, Y.; Wang, Z.; Feng, J.; Yan, S.; Zhang, H.; Li, Z.; Zou, Z. Improvement in photocatalytic H<sub>2</sub> evolution over g-C<sub>3</sub>N<sub>4</sub> prepared from protonated melamine. *Appl. Surf. Sci.* 2014, 295, 253–259.
58. Zhang, J.; Sun, J.; Maeda, K.; Domen, K.; Liu, P.; Antonietti, M.; Fu, X.; Wang, X. Sulfur-mediated synthesis of carbon nitride: Band-gap engineering and improved functions for photocatalysis. *Energy Environ. Sci.* 2011, 4, 675–678.
59. Gong, X.-Q.; Selloni, A.; Batzill, M.; Diebold, U. Steps on anatase TiO<sub>2</sub>(101). *Nat. Mater.* 2006, 5, 665–670.
60. Nowotny, M.K.; Sheppard, L.R.; Bak, T.; Nowotny, J. Defect chemistry of titanium dioxide. application of defect engineering in processing of TiO<sub>2</sub>-based photocatalysts. *J. Phys. Chem. C* 2008, 112, 5275–5300.
61. Hong, Z.; Shen, B.; Chen, Y.; Lin, B.; Gao, B. Enhancement of photocatalytic H<sub>2</sub> evolution over nitrogen-deficient graphitic carbon nitride. *J. Mater. Chem. A* 2013, 1, 11754–11761.
62. Lau, V.W.-H.; Mesch, M.B.; Duppel, V.; Blum, V.; Senker, J.; Lotsch, B.V. Low-Molecular-Weight Carbon Nitrides for Solar Hydrogen Evolution. *J. Am. Chem. Soc.* 2015, 137, 1064–1072.
63. Niu, P.; Liu, G.; Cheng, H.-M. Nitrogen Vacancy-Promoted Photocatalytic Activity of Graphitic Carbon Nitride. *J. Phys. Chem. C* 2012, 116, 11013–11018.
64. Liu, J.; Wang, H.; Chen, Z.P.; Moehwald, H.; Fiechter, S.; van de Krol, R.; Wen, L.; Jiang, L.; Antonietti, M. Microcontact-Printing-Assisted Access of Graphitic Carbon Nitride Films with Favorable Textures toward Photoelectrochemical Application. *Adv. Mater.* 2015, 27, 712–718.
65. Yang, Z.; Zhang, Y.; Schnepf, Z. Soft and hard templating of graphitic carbon nitride. *J. Mater. Chem. A* 2015, 3, 14081–14092.
66. Tong, Z.; Yang, D.; Li, Z.; Nan, Y.; Ding, F.; Shen, Y.; Jiang, Z. Thylakoid-Inspired Multishell g-C<sub>3</sub>N<sub>4</sub> Nanocapsules with Enhanced Visible-Light Harvesting and Electron Transfer Properties for High-Efficiency Photocatalysis. *ACS Nano* 2017, 11, 1103–1112.
67. Ong, W.-J.; Tan, L.-L.; Ng, Y.H.; Yong, S.-T.; Chai, S.-P. Graphitic Carbon Nitride (g-C<sub>3</sub>N<sub>4</sub>)-Based Photocatalysts for Artificial Photosynthesis and Environmental Remediation: Are We a Step Closer To Achieving Sustainability? *Chem.*

68. Dong, G.; Zhang, Y.; Pan, Q.; Qiu, J. A fantastic graphitic carbon nitride (g-C<sub>3</sub>N<sub>4</sub>) material: Electronic structure, photocatalytic and photoelectronic properties. *J. Photochem. Photobiol. C-Photochem. Rev.* 2014, 20, 33–50.
69. Li, M.; Zhang, L.; Wu, M.; Du, Y.; Fan, X.; Wang, M.; Zhang, L.; Kong, Q.; Shi, J. Mesostructured CeO<sub>2</sub>/g-C<sub>3</sub>N<sub>4</sub> nanocomposites: Remarkably enhanced photocatalytic activity for CO<sub>2</sub> reduction by mutual component activations. *Nano Energy* 2016, 19, 145–155.
70. Dong, J.; Zhang, Y.; Hussain, M.I.; Zhou, W.; Chen, Y.; Wang, L.-N. g-C<sub>3</sub>N<sub>4</sub>: Properties, Pore Modifications, and Photocatalytic Applications. *Nanomaterials* 2022, 12, 121.
71. Zhao, S.; Zhang, Y.; Zhou, Y.; Wang, Y.; Qiu, K.; Zhang, C.; Fang, J.; Sheng, X. Facile one-step synthesis of hollow mesoporous g-C<sub>3</sub>N<sub>4</sub> spheres with ultrathin nanosheets for photoredox water splitting. *Carbon* 2018, 126, 247–256.
72. Hu, R.; Wang, X.; Dai, S.; Shao, D.; Hayat, T.; Alsaedi, A. Application of graphitic carbon nitride for the removal of Pb(II) and aniline from aqueous solutions. *Chem. Eng. J.* 2015, 260, 469–477.
73. Zhang, Y.; Schnepp, Z.; Cao, J.; Ouyang, S.; Li, Y.; Ye, J.; Liu, S. Biopolymer-Activated Graphitic Carbon Nitride towards a Sustainable Photocathode Material. *Sci. Rep.* 2013, 3, 2163.
74. Xu, J.; Wang, Y.; Zhu, Y. Nanoporous Graphitic Carbon Nitride with Enhanced Photocatalytic Performance. *Langmuir* 2013, 29, 10566–10572.
75. Shalom, M.; Inal, S.; Fettkenhauer, C.; Neher, D.; Antonietti, M. Improving Carbon Nitride Photocatalysis by Supramolecular Preorganization of Monomers. *J. Am. Chem. Soc.* 2013, 135, 7118–7121.
76. Zhang, M.; Yan, X.; Huang, F.; Niu, Z.; Gibson, H.W. Stimuli-Responsive Host-Guest Systems Based on the Recognition of Cryptands by Organic Guests. *Acc. Chem. Res.* 2014, 47, 1995–2005.
77. Cui, Q.; Xu, J.; Wang, X.; Li, L.; Antonietti, M.; Shalom, M. Phenyl-Modified Carbon Nitride Quantum Dots with Distinct Photoluminescence Behavior. *Angew. Chem.-Int. Ed.* 2016, 55, 3672–3676.
78. Bhunia, M.K.; Yamauchi, K.; Takanaabe, K. Harvesting Solar Light with Crystalline Carbon Nitrides for Efficient Photocatalytic Hydrogen Evolution. *Angew. Chem.-Int. Ed.* 2014, 53, 11001–11005.
79. Jordan, T.; Fechler, N.; Xu, J.; Brenner, T.J.K.; Antonietti, M.; Shalom, M. “Caffeine Doping” of Carbon/Nitrogen-Based Organic Catalysts: Caffeine as a Supramolecular Edge Modifier for the Synthesis of Photoactive Carbon Nitride Tubes. *Chemcatchem* 2015, 7, 2826–2830.
80. Gao, J.; Wang, J.; Qian, X.; Dong, Y.; Xu, H.; Song, R.; Yan, C.; Zhu, H.; Zhong, Q.; Qian, G.; et al. One-pot synthesis of copper-doped graphitic carbon nitride nanosheet by heating Cu-melamine supramolecular network and its enhanced visible-light-driven photocatalysis. *J. Solid State Chem.* 2015, 228, 60–64.
81. Chen, Z.P.; Antonietti, M.; Dontsova, D. Enhancement of the Photocatalytic Activity of Carbon Nitrides by Complex Templating. *Chem. A Eur. J.* 2015, 21, 10805–10811.
82. Shalom, M.; Guttentag, M.; Fettkenhauer, C.; Inal, S.; Neher, D.; Llobet, A.; Antonietti, M. In Situ Formation of Heterojunctions in Modified Graphitic Carbon Nitride: Synthesis and Noble Metal Free Photocatalysis. *Chem. Mater.* 2014, 26, 5812–5818.
83. Fan, X.; Xing, Z.; Shu, Z.; Zhang, L.; Wang, L.; Shi, J. Improved photocatalytic activity of g-C<sub>3</sub>N<sub>4</sub> derived from cyanamide-urea solution. *RSC Adv.* 2015, 5, 8323–8328.
84. Shalom, M.; Gimenez, S.; Schipper, F.; Herraiz-Cardona, I.; Bisquert, J.; Antonietti, M. Controlled Carbon Nitride Growth on Surfaces for Hydrogen Evolution Electrodes. *Angew. Chem.-Int. Ed.* 2014, 53, 3654–3658.
85. Bai, X.; Wang, L.; Zong, R.; Zhu, Y. Photocatalytic Activity Enhanced via g-C<sub>3</sub>N<sub>4</sub> Nanoplates to Nanorods. *J. Phys. Chem. C* 2013, 117, 9952–9961.
86. Wang, S.; Li, C.; Wang, T.; Zhang, P.; Li, A.; Gong, J. Controllable synthesis of nanotube-type graphitic C<sub>3</sub>N<sub>4</sub> and their visible-light photocatalytic and fluorescent properties. *J. Mater. Chem. A* 2014, 2, 2885–2890.
87. Chen, D.; Wang, K.; Xiang, D.; Zong, R.; Yao, W.; Zhu, Y. Significantly enhancement of photocatalytic performances via core-shell structure of ZnO@mpg-C<sub>3</sub>N<sub>4</sub>. *Appl. Catal. B-Environ.* 2014, 147, 554–561.
88. Cheng, F.; Wang, H.; Dong, X. The amphoteric properties of g-C<sub>3</sub>N<sub>4</sub> nanosheets and fabrication of their relevant heterostructure photocatalysts by an electrostatic re-assembly route. *Chem. Commun.* 2015, 51, 17176–17179.
89. Schwinghammer, K.; Mesch, M.B.; Duppel, V.; Ziegler, C.; Senker, J.; Lotsch, B.V. Crystalline Carbon Nitride Nanosheets for Improved Visible-Light Hydrogen Evolution. *J. Am. Chem. Soc.* 2014, 136, 1730–1733.
90. Liu, G.; Wang, T.; Zhang, H.; Meng, X.; Hao, D.; Chang, K.; Li, P.; Kako, T.; Ye, J. Nature-Inspired Environmental “Phosphorylation” Boosts Photocatalytic H<sub>2</sub> Production over Carbon Nitride Nanosheets under Visible-Light Irradiation.

91. Niu, P.; Zhang, L.; Liu, G.; Cheng, H.-M. Graphene-Like Carbon Nitride Nanosheets for Improved Photocatalytic Activities. *Adv. Funct. Mater.* 2012, 22, 4763–4770.
92. Yang, S.; Gong, Y.; Zhang, J.; Zhan, L.; Ma, L.; Fang, Z.; Vajtai, R.; Wang, X.; Ajayan, P.M. Exfoliated Graphitic Carbon Nitride Nanosheets as Efficient Catalysts for Hydrogen Evolution under Visible Light. *Adv. Mater.* 2013, 25, 2452–2456.
93. Zhao, H.; Yu, H.; Quan, X.; Chen, S.; Zhang, Y.; Zhao, H.; Wang, H. Fabrication of atomic single layer graphitic-C<sub>3</sub>N<sub>4</sub> and its high performance of photocatalytic disinfection under visible light irradiation. *Appl. Catal. B-Environ.* 2014, 152, 46–50.
94. Yin, Y.; Han, J.; Zhang, X.; Zhang, Y.; Zhou, J.; Muir, D.; Sutarto, R.; Zhang, Z.; Liu, S.; Song, B. Facile synthesis of few-layer-thick carbon nitride nanosheets by liquid ammonia-assisted lithiation method and their photocatalytic redox properties. *RSC Adv.* 2014, 4, 32690–32697.
95. Ma, L.; Fan, H.; Li, M.; Tian, H.; Fang, J.; Dong, G. A simple melamine-assisted exfoliation of polymeric graphitic carbon nitrides for highly efficient hydrogen production from water under visible light. *J. Mater. Chem. A* 2015, 3, 22404–22412.
96. Xu, H.; Yan, J.; She, X.; Xu, L.; Xia, J.; Xu, Y.; Song, Y.; Huang, L.; Li, H. Graphene-analogue carbon nitride: Novel exfoliation synthesis and its application in photocatalysis and photoelectrochemical selective detection of trace amount of Cu<sup>2+</sup>. *Nanoscale* 2014, 6, 1406–1415.
97. Ma, L.; Fan, H.; Wang, J.; Zhao, Y.; Tian, H.; Dong, G. Water-assisted ions in situ intercalation for porous polymeric graphitic carbon nitride nanosheets with superior photocatalytic hydrogen evolution performance. *Appl. Catal. B Environ.* 2016, 190, 93–102.
98. Zhou, L.; Zhang, H.; Sun, H.; Liu, S.; Tade, M.O.; Wang, S.; Jin, W. Recent advances in non-metal modification of graphitic carbon nitride for photocatalysis: A historic review. *Catal. Sci. Technol.* 2016, 6, 7002–7023.
99. Zhou, L.; Feng, J.; Qiu, B.; Zhou, Y.; Lei, J.; Xing, M.; Wang, L.; Zhou, Y.; Liu, Y.; Zhang, J. Ultrathin g-C<sub>3</sub>N<sub>4</sub> nanosheet with hierarchical pores and desirable energy band for highly efficient H<sub>2</sub>O<sub>2</sub> production. *Appl. Catal. B-Environ.* 2020, 267, 118396.
100. Tang, C.; Cheng, M.; Lai, C.; Li, L.; Yang, X.; Du, L.; Zhang, G.; Wang, G.; Yang, L. Recent progress in the applications of non-metal modified graphitic carbon nitride in photocatalysis. *Coord. Chem. Rev.* 2023, 474, 214846.
101. Sudhaik, A.; Raizada, P.; Shandilya, P.; Jeong, D.-Y.; Lim, J.-H.; Singh, P. Review on fabrication of graphitic carbon nitride based efficient nanocomposites for photodegradation of aqueous phase organic pollutants. *J. Ind. Eng. Chem.* 2018, 67, 28–51.
102. Nasir, M.S.; Yang, G.; Ayub, I.; Wang, S.; Wang, L.; Wang, X.; Yan, W.; Peng, S.; Ramakarishna, S. Recent development in graphitic carbon nitride based photocatalysis for hydrogen generation. *Appl. Catal. B-Environ.* 2019, 257, 117855.
103. Hayat, A.; Syed, J.A.S.G.; Al-Sehemi, A.S.; El-Nasser, K.; Taha, T.A.A.; Al-Ghamdi, A.A.; Amin, M.; Ajmal, Z.; Iqbal, W.; Palamanit, A.; et al. State of the art advancement in rational design of g-C<sub>3</sub>N<sub>4</sub> photocatalyst for efficient solar fuel transformation, environmental decontamination and future perspectives. *Int. J. Hydrogen Energy* 2022, 47, 10837–10867.
104. Zeng, Y.; Liu, X.; Liu, C.; Wang, L.; Xia, Y.; Zhang, S.; Luo, S.; Pei, Y. Scalable one-step production of porous oxygen-doped g-C<sub>3</sub>N<sub>4</sub> nanorods with effective electron separation for excellent visible-light photocatalytic activity. *Appl. Catal. B-Environ.* 2018, 224, 1–9.
105. Wen, J.; Zhou, L.; Tang, Q.; Xiao, X.; Sun, S. Photocatalytic degradation of organic pollutants by carbon quantum dots functionalized g-C<sub>3</sub>N<sub>4</sub>: A review. *Ecotoxicol. Environ. Saf.* 2023, 262, 115133.
106. Wang, Y.; Zhong, S.; Niu, Z.; Dai, Y.; Li, J. Synthesis and up-to-date applications of 2D microporous g-C<sub>3</sub>N<sub>4</sub> nanomaterials for sustainable development. *Chem. Commun.* 2023, 59, 10883–10911.
107. Truong, H.B.; Hur, J.; Nguyen, X.C. Recent advances in g-C<sub>3</sub>N<sub>4</sub>-based photocatalysis for water treatment: Magnetic and floating photocatalysts, and applications of machine-learning techniques. *J. Environ. Manag.* 2023, 345, 118895.
108. Ding, M.; Wei, Z.; Zhu, X.; Liu, D. Effect of Different g-C<sub>3</sub>N<sub>4</sub> Content on Properties of NiCo<sub>2</sub>S<sub>4</sub>/g-C<sub>3</sub>N<sub>4</sub> Composite as Electrode Material for Supercapacitor. *Int. J. Electrochem. Sci.* 2022, 17, 22121.
109. Chen, X.; Shi, R.; Chen, Q.; Zhang, Z.; Jiang, W.; Zhu, Y.; Zhang, T. Three-dimensional porous g-C<sub>3</sub>N<sub>4</sub> for highly efficient photocatalytic overall water splitting. *Nano Energy* 2019, 59, 644–650.
110. Fu, J.; Zhu, B.; Jiang, C.; Cheng, B.; You, W.; Yu, J. Hierarchical Porous O-Doped g-C<sub>3</sub>N<sub>4</sub> with Enhanced Photocatalytic CO<sub>2</sub> Reduction Activity. *Small* 2017, 13, 1603938.

111. Dou, M.; Wang, J.; Gao, B.; Xu, C.; Yang, F. Photocatalytic difference of amoxicillin and cefotaxime under visible light by mesoporous g-C<sub>3</sub>N<sub>4</sub>: Mechanism, degradation pathway and DFT calculation. *Chem. Eng. J.* 2020, 383, 123134.
- 

Retrieved from <https://encyclopedia.pub/entry/history/show/121938>